Three-Dimensional Structure of the R115E Mutant of T4-Bacteriophage 2′-Deoxycytidylate Deaminase[†,‡]

Rami Almog, Frank Maley, Gladys F. Maley, Robert MacColl, and Patrick Van Roey*

Wadsworth Center, New York State Department of Health, Albany, New York 12201-0509

Received May 25, 2004; Revised Manuscript Received August 27, 2004

ABSTRACT: 2′-Deoxycytidylate deaminase (dCD) converts deoxycytidine 5′-monophosphate (dCMP) to deoxyuridine 5′-monophosphate and is a major supplier of the substrate for thymidylate synthase, an important enzyme in DNA synthesis and a major target for cancer chemotherapy. Wild-type dCD is allosterically regulated by the end products of its metabolic pathway, deoxycytidine 5′-triphosphate and deoxythymidine 5′-triphosphate, which act as an activator and an inhibitor, respectively. The first crystal structure of a dCD, in the form of the R115E mutant of the T4-bacteriophage enzyme complexed with the active site inhibitor pyrimidin-2-one deoxyribotide, has been determined at 2.2 Å resolution. This mutant of dCD is active, even in the absence of the allosteric regulators. The molecular topology of dCD is related to that of cytidine deaminase (CDA) but with modifications for formation of the binding site for the phosphate group of dCMP. The enzyme has a zinc ion-based mechanism that is similar to that of CDA. A second zinc ion that is present in bacteriophage dCD, but absent in mammalian dCD and CDA, is important for the structural integrity of the enzyme and for the binding of the phosphate group of the substrate or inhibitor. Although the R115E mutant of dCD is a dimer in solution, it crystallizes as a hexamer, mimicking the natural state of the wild-type enzyme. Residues 112 and 115, which are known to be important for the binding of the allosteric regulators, are found in a pocket that is at the intersubunit interfaces in the hexamer but distant from the substrate-binding site. The substrate-binding site is composed of residues from a single protein molecule and is sequestered in a deep groove. This groove is located at the outer surface of the hexamer but ends at the subunit interface that also includes residue 115. It is proposed that the absence of subunit interactions at this interface in the dimeric R115E mutant renders the substrate-binding site accessible. In contrast, for the wild-type enzyme, binding of dCTP induces an allosteric effect that affects the subunit interactions and results in an increase in the accessibility of the binding site.

2′-Deoxycytidylate deaminase (dCD)[1] converts deoxycytidine 5′-monophosphate (dCMP) (Figure 1a) to deoxyuridine 5′-monophosphate (dUMP), the substrate of thymidylate synthase (TS) (*1*). dCD has been shown to be a major, although not exclusive, provider of dUMP (*2*), while TS is the only *de novo* source of deoxythymidine 5′-monophosphate (dTMP) in most biological systems. Consequently, TS is essential for DNA synthesis and is thus a target for anticancer agents (*3*, *4*). In addition to processing successive steps in dTMP synthesis, TS and dCD also appear to have a biological relationship, in that their levels are simultaneously elevated in rapidly dividing cells while they are minimally active in nondividing cells (*5*). dCD also has been shown to reduce the efficiency of anticancer and antiviral drugs, such as cytosine arabinoside, by deamination at the nucleotide level (*6*, *7*), but it can potentiate the activity of other drugs such as 5-fluorodeoxycytidine (*8*). Together, these properties of dCD suggest that inhibitors of dCD have potential applications in chemotherapy, warranting structure−function studies of the enzyme and structure-based development of dCD inhibitors.

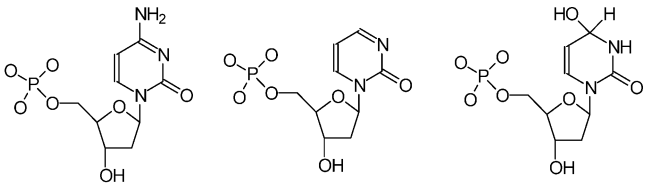

FIGURE 1: Schematic diagram of dCD ligands observed in the crystal structure: (a) substrate, 2′-deoxycytidine 5′-monophosphate; (b) inhibitor, PdR; and (c) intermediate analogue, 3,4-dihydrouridine 5′-monophosphate.

dCD is present in most eukaryotic and bacterial organisms, with the exception of the enteric bacteria *Escherichia coli* and *Salmonella typhimurium*, which apparently employ a deoxycytidine 5′-triphosphate (dCTP) deaminase to maintain the balance between dCTP and dTTP in the cell (*9*). Among dCDs, those from humans and T4-bacteriophage have been studied most extensively and have been shown to represent

[†] The X-ray diffraction facilities of beamline X12c of the National Synchrotron Light Source are supported by grants from the DOE and the NIH.

[‡] The atomic coordinates and observed structure factors have been deposited in the Protein Data Bank as entry 1TEO.

* To whom correspondence should be addressed: Wadsworth Center, P.O. Box 509, Albany, NY 12201-0509. Phone: (518) 474-1444. Fax: (518) 408-2190. E-mail: vanroey@wadsworth.org.

[1] Abbreviations: CDA, cytidine deaminase; dCD, 2′-deoxycytidylate deaminase; PdR, pyrimidin-2-one deoxyribotide.

10.1021/bi048928h CCC: $27.50
Published on Web 10/09/2004

two distinct classes of the enzyme. Both enzymes are active as homohexamers, in which the active sites of all six subunits sites are identical, and all six sites are apparently active (*10*). This differs from TS, which is dimeric but a half-of-the-sites-activity enzyme (*11*, *12*). Mammalian dCDs contain a single zinc ion per monomer that is required for catalytic activity. In contrast, the bacteriophage enzymes contain two zinc ions per monomer that are both required for activity, although only one appears to be involved in the catalytic mechanism. Four cysteines (19, 49, 132, and 135) and two histidines (94 and 104) have been identified as being important for zinc binding in T4-dCD (G. F. Maley and R. Ketring, unpublished observations). Cys132, Cys135, and His104 form one zinc-binding site which, based on sequence analysis, corresponds to the Cys110, Cys113, and His84 site of the human enzyme and therefore forms the binding site for the catalytic zinc ion. Cys19, Cys49, and His94 (*13*) are part of the binding site for the second zinc ion. Mutagenesis of these residues results in the loss of one zinc ion and of enzyme activity. Interestingly, mutagenesis of adjacent cysteines, Cys20 and Cys50, does not affect dCD activity.

The most unusual property of dCD is its allosteric regulation by the end products of its metabolic pathway, dCTP and deoxythymidine 5′-triphosphate (dTTP). The enzyme is activated by dCTP and inhibited by dTTP, providing a unique means by which to balance the availability of the pyrimidine nucleotides for DNA synthesis (*1*, *5*). The degree of dependence on the regulators differs between the mammalian and bacteriophage forms of the enzyme. T4-bacteriophage dCD is completely dependent on the presence of dCTP for activity, while the human enzyme is weakly active at low substrate concentrations, in the absence of the activator (*14*). The inhibitor and activator appear to bind at the same site, which is thought to be distant from the active site, and to act through an allosteric mechanism that involves changes in the subunit interactions of the hexameric functional form of the enzyme (*5*, *10*). Residues Phe112 and Arg115 of T4-phage dCD have been implicated in the binding of the allosteric regulators (*14*, *15*). Photofixation experiments showed that dTTP binding involves stacking of the pyrimidine ring with the side chain of Phe112, an effect that is impaired in the presence of dCTP (*15*). The importance of this interaction with Phe112 was confirmed by site-directed mutagenesis experiments. The Ala mutation of Phe112 (F112A) yields a protein that is active, at ∼10% of the level of wild-type T4-phage dCD, but one that is essentially independent of the allosteric regulators (*15*). Similarly, the R115E mutant of T4-bacteriophage dCD has a specific activity that is ∼60% of that of the wild-type enzyme, is independent of dCTP activation or dTTP inhibition, and, most interestingly, is functional in solution as a dimer (*16*). These results indicate that there is a relationship between the oligomeric state of dCD and its regulation by dCTP and dTTP, and they also imply that the allosteric regulation involves conformational changes at the intersubunit interface. However, the exact nature of these changes, and how these effects influence the enzymatic activity of wild-type dCD, remain unknown.

dCD is related to cytidine deaminase (CDA), which catalyzes the same reaction, but for the unphosphorylated substrate. This enzyme has been studied extensively, both structurally and functionally (*17*−*19*). dCD and CDA show significant similarities in two sequence segments that correspond to residues 24−41 and 104−144 of T4-bacteriophage dCD (*20*). The second segment includes the residues that form the catalytic site, suggesting similarities in the catalytic mechanisms of the two enzymes. This is further supported by the fact that dCD is inhibited by compounds that are 5′-monophosphate derivatives of CDA inhibitors. The crystal structures of two forms of CDA have been reported: a dimeric form (CDA-D) from *E. coli* (*17*) and a tetrameric form (CDA-T) from *Bacillis subtilis* (*21*). However, unlike dCD, neither form of CDA is allosterically regulated. Studies of the catalytic mechanism of CDA-D have shown that the catalytic site contains a zinc ion that is coordinated by two cysteines, one histidine, and a water molecule. This zinc ion activates the water molecule, which, as a hydroxyl, reacts with C4 of the cytidine. A nearby glutamic acid interacts with N3 of the cytidine, functioning as a proton donor in the initial step and a proton acceptor in the final step of the reaction. The active site of CDA-T is similar to that of CDA-D, except that its zinc ion is coordinated by three cysteines and a water molecule. Charge-difference effects due to the histidine-to-cysteine substitution are reportedly offset by second-order interactions (*21*, *22*).

Here, we report the first three-dimensional structure of a dCD, in the form of a complex of the R115E mutant of T4-bacteriophage dCD (T4-dCD-R115E) with the inhibitor pyrimidin-2-one deoxyribotide (PdR) (Figure 1b). This mutant was selected for these structural studies because it can be obtained in a monodisperse state and because it has better solubility properties than the wild-type enzyme. The structure reveals several important aspects of the catalytic mechanism and substrate binding characteristics, as well as the role of the noncatalytic zinc ion. It allows us to propose a hypothesis for the activity of the mutant as a dimer, and it suggests a model for the mechanism for the allosteric regulation of the wild-type enzyme.

MATERIALS AND METHODS

Protein Expression and Purification. T4-dCD-R115E was cloned into the pET-3c vector, expressed in *E. coli* (*16*), and purified as previously described (*23*). Under these conditions, at least 20 mg of pure protein is obtained from a 1 L culture. The R115E mutant was obtained using the Quikchange procedure (Stratagene, La Jolla, CA).

Quaternary Structure Determination. Analytical centrifuge experiments for T4-dCD-R115E were performed using a Beckman XLI analytical ultracentrifuge and an AN-60-Ti rotor at 25 °C. The protein samples were dialyzed into a buffer consisting of 0.050 M potassium phosphate (pH 7.0). The viscosity and density of the buffers and the partial specific volume of the protein were obtained from SEDNTERP, which is public domain software developed by Laue and others (*24*). The partial specific volume (v-bar) was calculated from the protein's amino acid content to be 0.74 mL/g at 25 °C.

For the sedimentation velocity studies, the sample volume was 0.420 mL and the reference volume of the dialysis buffer was 0.440 mL. Protein samples at concentrations of 0.2, 0.5, 1.0, and 5.2 mg/mL were run at 50 000 rpm in an aluminum-filled Epon two-sector centerpiece with quartz windows.

Table 1: Data Collection and Refinement Statistics[a]

Data Collection			
	inflection	peak	remote
wavelength (Å)	1.286	1.2809	1.000
redundancy	9.7	10.3	10.8
completeness (%)	99.9 (99.7)	99.9 (99.8)	99.9 (99.9)
$\langle I/\sigma(I)\rangle$	21.3 (3.1)	20.6 (2.6)	17.8 (2.8)
R_{mer}	0.044 (0.489)	0.050 (0.441)	0.045 (0.412)

Refinement	
no. of reflections	15506
R_{cryst}	0.216
R_{free}	0.244
rmsd from ideality	
bond lengths (Å)	0.006
bond angles (deg)	1.15
dihedrals (deg)	23.5
average *B*-factors (Å^2)	
protein	38.2
zinc ions (2)	34.3
inhibitor	41.5
water (47)	41.2

[a] Values in parentheses are for the highest-resolution shell (2.3−2.2 Å).

Detection by absorption optics was at 280 nm for the three lower concentrations, and 300 nm for the most concentrated sample. The data were analyzed by the c(s) method found in Sedfit, a program developed by Schuck and co-workers (*25*). The experimentally calculated sedimentation coefficients from Sedfit were converted to $s_{20,w}$ by multiplication of the experimentally obtained value by 0.92, a factor that was calculated from the standard equation.

Crystallization. T4-dCD-R115E was crystallized in the presence of the inhibitor PdR, which was prepared as previously described (*14*). The protein solution containing 0.28 mM T4-dCD-R115E, 0.02 M phosphate (pH 7.2), 0.38 mM PdR, and 30 mM DTT was mixed with an equal volume of the precipitation buffer [1.3 M $(NH_4)_2SO_4$, 0.1 M sodium citrate (pH 6.0), and 10 mM DTT] and was equilibrated against the latter solution in hanging-drop vapor-diffusion experiments at 22 °C. The crystals grew after 3 weeks and belong to space group $P6_322$, with the following cell parameters: $a = b = 114.5$ Å and $c = 76.9$ Å. There is one monomer in the asymmetric unit with a V_M of 3.44 Da/Å^3 and a solvent content of 64%. The crystals were flash-cooled in the cold nitrogen stream after addition of 20% glycerol to the mother liquor. All diffraction data were measured at 100 K.

Structure Determination and Refinement. The structure was determined by multiwavelength anomalous diffraction methods using the anomalous scattering of the zinc ion for phasing. Three-wavelength X-ray diffraction data to 2.2 Å resolution were measured at beamline X12c of the National Synchrotron Light Source (Brookhaven National Laboratory, Upton, NY). Initial phases were obtained using SOLVE (*26*). After solvent flattening, using DM (*27*), the electron density map showed interpretable density for ~80% of the molecule. The model was built using TURBO-FRODO (*28*) and O (*29*), and was refined using CNS (*30*). Final R and R_{free} values are 0.220 and 0.247, respectively. The data collection and refinement statistics are listed in Table 1. Ninety-six percent of the non-glycine residues are in the most favored region, and the remaining 4% are in the additionally allowed region of the Ramachandran plot (*31*). Figure 2 shows the final electron density map for the inhibitor.

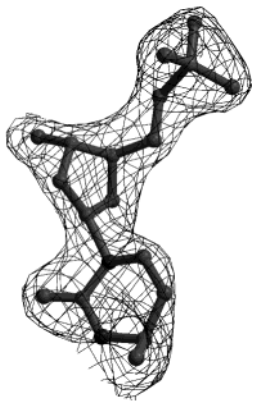

FIGURE 2: Final $2F_o - F_c$ electron density map for the inhibitor contoured at the 1.5σ level. This figure was prepared with BOBSCRIPT (*42*).

RESULTS

Molecular and Quaternary Structure of T4-dCD-R115E. The three-dimensional structure of T4-dCD-R115E was determined by MAD phasing methods and was refined at 2.2 Å resolution. The final model (Figure 3a) includes residues 1−62 and 84−193 of the 193-residue molecule. The absence of electron density for residues 63−83 indicates that these residues form a highly flexible loop that is disordered in the crystal. T4-dCD-R115E has an α/β-fold consisting of a central five-stranded mixed β-sheet that is flanked by the N-terminal α-helix and a long loop on one face, four α-helices on the opposite face, and a sixth α-helix along one edge.

Although T4-dCD-R115E was shown to be a dimer in solution by gel filtration analysis (*16*), the crystal structure contains a hexamer, or a trimer of dimers, that has 32 symmetry (Figure 3b) with two distinct subunit interfaces. The subunit interface between molecules A and B (hereafter called interface AB) consists of a central antiparallel two-helix bundle formed by the N-terminal α-helices of the two subunits, surrounded by interacting loops. The subunit interactions at the other interface (AC) are more complex, and involve contacts between loops that join the α-helices and β-strands on the opposite face of the subunit, most importantly, the loops following helices α3−α5. The two interfaces have interaction areas with similar dimensions, with total buried surface areas of 2593 and 2352 Å^2 for interfaces AB and AC, respectively. Interestingly, the residues that are known to be important for allosteric regulation, 112 and 115, are found at the interfaces and are close to the core of the hexamer.

Sedimentation velocity experiments were performed to complement the earlier gel filtration experiments and to confirm that T4-dCD-R115E is a dimer in solution. The protein was examined at loading concentrations ranging from 0.2 to 5.2 g/L. Data analysis by the c(s) method in Sedfit (*25*) showed the presence of a single component at all concentrations. When extrapolated to a zero concentration, the $s_{20,w}$ was found to be 3.55 S. The plot of the sedimentation coefficient ($s_{20,w}$) versus concentration gave an indication of a single component that was quite stable in this concentration

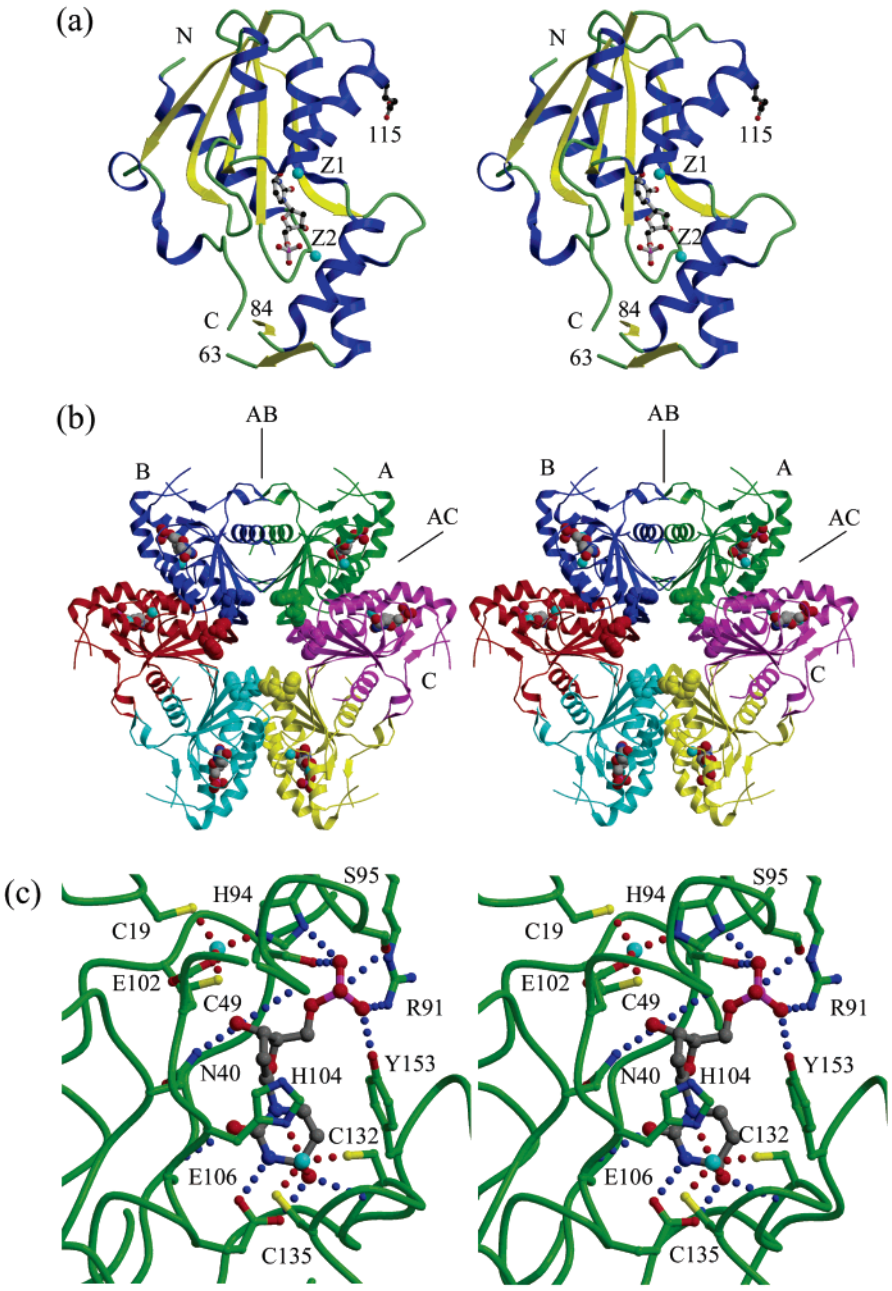

FIGURE 3: (a) Three-dimensional structure of T4-dCD-R115E with the inhibitor bound. Z1 denotes the catalytically essential zinc ion, while Z2 denotes the second zinc ion. Residue 115 is shown to illustrate the relative locations of the active site and the allosteric regulator-binding site. (b) Structure of the hexamer of T4-dCD-R115E as observed in the crystal. The six molecules that are shown are related by crystallographic symmetry and are therefore identical. Molecules A−C as referenced in the text are shown in green, blue, and magenta, respectively. The inhibitor bound in the active site is shown in multicolor CPK representation. The side chains of residues 112 and 115 of each molecule are shown in CPK representation in the same color as the corresponding backbone. (c) Detailed image of the substrate-binding site, zinc ion locations and coordinations, and protein−inhibitor interactions. Contacts with the zinc ions are shown as red dotted lines. Protein−inhibitor hydrogen bonds are shown as blue dotted lines. This figure was prepared with MOLSCRIPT (*43*) and RASTER3D (*44*).

range. The value of 3.55 S is consistent with the presence of a dimeric oligomer and compares to an $s_{20,w}$ value of ~6 S that was previously obtained for wild-type T2-bacteriophage dCD, which is hexameric (*32*).

Distinct Roles of the Zinc Ions. The two zinc ions are located at opposite ends of the substrate-binding site occupied by the inhibitor. One zinc ion is tetrahedrally coordinated by His104, Cys132, Cys135, and the O4 hydroxyl of the inhibitor and is clearly the catalytically important cation (Figure 3c). His104 is located at the N-terminus of helix α4, while Cys132 and Cys135 are part of the N-terminal turn of helix α5. The second zinc ion is also found in a tetrahedral cluster formed by Cys19, Cys49, His94, and Glu102. This zinc ion is located near the surface of the substrate-binding site but is not solvent-exposed, and it does not interact directly with the inhibitor. It joins the loop between helix α1 and strand β1 (residues 17−21) with helices α2 (residues 48−56) and α3 (90−102), shaping the binding site of the phosphate group of the inhibitor, which is in hydrogen bonding contact with Ser21, Arg91, His94, and Ser95. In addition, the zinc ion is involved in compensating for the negative charge of the phosphate group, through the bridging

interactions of His94. Thus, it appears that this zinc ion does not play a direct role in catalysis, but rather, it appears to have a role in substrate binding, in addition to being structurally important. It may also play a role in defining the conformation of the protein at the subunit interface, because residues of the loop joining strand β2 with helix α2 as well as some residues in helix α3 participate in subunit interactions at the same interface at which residue 115 does.

Substrate-Binding Site. The $F_o - F_c$ difference electron density maps showed clear density for the inhibitor in a cavity located above strand β1 and defined at the catalytic site by the N-termini of helices α4 and α5, and at the binding site of the phosphate group by the edge of helix α3. The PdR inhibitor is observed as its hydrated derivative, 3,4-dihydrouridine 5′-monophosphate (Figures 1c and 3c), which is an analogue of the reaction intermediate in which C4 is hydroxylated. In addition to the contact with the zinc ion through the C4 hydroxyl, the pyrimidine ring interacts with Ala105, Glu106, and Tyr153. The hydrogen bond between the carboxylate group of Glu106 and N3 of the pyrimidine confirms the role of the glutamic acid as a proton donor and/or acceptor. The side chain of Tyr153 is involved in a hydrophobic interaction by stacking against the C5−C6 edge of the base. This interaction appears to be important for substrate specificity. It blocks the binding of ligands that have substituents at C5, such as 5-hydroxymethyl-dCMP and dTMP. This structural detail is also consistent with earlier findings that increasing the size of the 5′-halogen substituent on dCMP derivatives reduces its activity as a substrate for T4-bacteriophage dCD, but not for the eukaryotic enzymes (*8*, *33*). Tyr153 is also involved in binding the phosphate group through a hydrogen bond between its hydroxyl and an oxygen atom of the phosphate group. The O3′ hydroxyl of the deoxyribose moiety is in hydrogen bonding contact with Cys19 and Asn40. The phosphate group occupies a positively charged pocket that consists of the side chains of Arg91, His94, Ser95, Tyr153, and Lys155. His94 appears to be especially important in compensating for the negative charge of the phosphate because it interacts with both the phosphate group and the second zinc ion.

The substrate-binding site is composed of residues from a single dCD molecule. It is located at the bottom of a long groove that extends over the outer surface of the molecule as it is incorporated into the hexamer. While the inhibitor itself is bound more than 10 Å from the subunit interfaces, one end of the groove and the flanking helices, α3 and α5, make contacts with the molecule across the AC interface (Figure 4). The inhibitor is buried deeply in the protein, with only 10 Å^2 of its surface accessible to a standard 1.4 Å solvent accessibility probe. Therefore, conformational flexibility is required for the substrate or products to enter or leave the active site. Such entrance or egress most likely involves an increase in the distance between helix α3 on one side and helix α5 and the loop (residues 150−158) joining strand β4 and helix α6 on the other side. In the hexamer observed in the crystal structure of T4-dCD-R115E, the subunit interactions across the AC interface appear to restrict the movement of α-helices 3 and 5. However, this form of the enzyme is a dimer in solution, most likely consisting of molecules A and B (see below), and thus lacks such restraints.

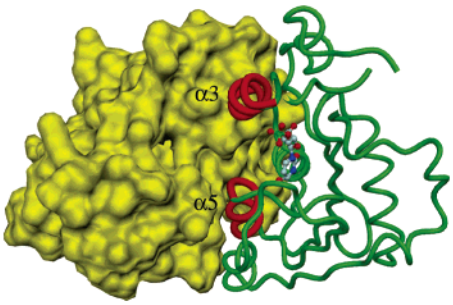

FIGURE 4: Subunit−subunit interactions. Interactions across the AC interface of the hexamer observed in the crystal structure. Molecule A is shown as a green ribbon representation with α-helices α3 and α5 highlighted in red. Molecule C is shown as a yellow surface representation. We propose that the interactions of α-helices α3 and α5 of molecule A with molecule C lock the enzyme in a closed conformation that does not allow substrate entry or egress. This figure was prepared with DINO (*45*).

Comparison between dCD and CDA. The crystal structures of several nucleoside and nucleotide deaminases have been reported, including those of cytosine deaminase (*34*), two distinct forms of CDA (*17*, *21*), and a bifunctional dCTP deaminase-dUTPase (*35*). Despite having very different folds, cytosine deaminase and CDA have similar, zinc ion-based, catalytic mechanisms. In contrast, the dCTP deaminase-dUTPase has a completely different mechanism that does not involve a metal ion.

dCD is most closely related, structurally as well as functionally, to CDA. Overall, the topology of the dCD monomer is similar to that of a monomer of CDA-T (Figure 5a). The β-sheet and three of the α-helices align well when superimposed. However, there are two major differences: (1) an insertion in dCD, residues 42−99, after the second β-strand that includes two α-helices (α2 and α3) and a long loop that is partially disordered and (2) an alternative folding of the molecule after the fourth β-strand that results in the fifth β-strand being in the opposite orientation. Thus, while in CDA β-strands 1−3 are antiparallel, 3 and 4 parallel, and 4 and 5 antiparallel, in dCD β-strands 1−3 are antiparallel and β-strands 3−5 parallel (Figure 5b). These two differences are important in shaping the binding site for the phosphate group of the substrate of dCD. Furthermore, because of differences in the quaternary structures, the substrate-binding sites are composed of different protein segments, although they have similar shapes and protein−ligand interactions. The dCD substrate-binding site is contained within a single monomer and is located on an exposed surface of the molecule. In contrast, multiple subunits of CDA interact to define its substrate-binding site, which is located at the interface between the subunits. CDA-D (*17*) is a dimeric enzyme in which each subunit consists of two domains that have similar folds, but in which the C-terminal domain lacks the active site residues. CDA-T (*21*) is a tetramer of four identical subunits that resemble the N-terminal domain of CDA-D, and with four complete active sites. The active sites of the CDAs consist of residues from three subunits (in the case of CDA-T) or of residues from both domains from one subunit and the N-terminal domain of the second subunit (in the case of CDA-D).

dCD and CDA exhibit significant similarities in two sequence segments that correspond to residues 24−41 and 104−144 of T4-bacteriophage dCD. The first segment

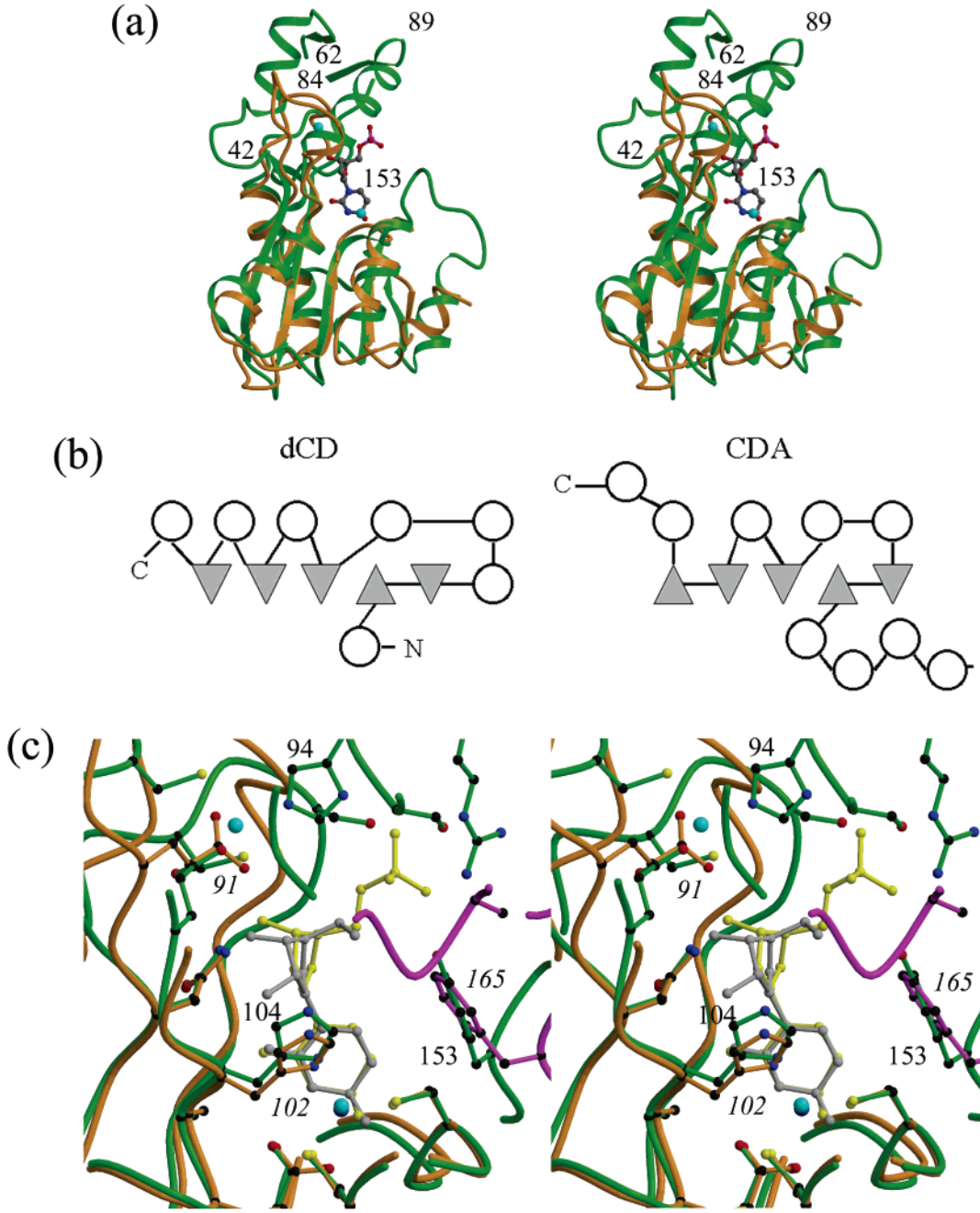

FIGURE 5: Topological relationship between dCD and CDA. (a) Superposition of a dCD monomer (green) with the catalytic domain of CDA-D (orange). The superposition was generated by least-squares fitting of five conserved secondary structure elements. The two main differences in the folds of the two proteins are the insertion in dCD after residue 42 (top) that forms most of the phosphate binding site and a difference in the fold after β-strand 4 (bottom right) that introduces a loop into dCD that includes Tyr153. (b) Schematic diagram of the topology differences between dCD and CDA. (c) Detailed view of the differences in the substrate-binding sites of dCD and CDA-D. The backbones and side chains are shown in green, orange, and magenta for dCD, the first molecule of CDA-D and the second CDA-D molecule, respectively. The dCD and CDA inhibitors are shown in yellow and light gray, respectively. Residue labels of dCD are displayed in regular type and those of CDA in italic type. Panels a and c were prepared with MOLSCRIPT (*43*) and RASTER3D (*44*).

corresponds to strand β1, which forms the core of the substrate-binding site, while the latter segment includes not only the residues that form the catalytic sites of both enzymes but also the residues known to be involved in the binding of the allosteric regulators of T4-dCD. The 1.6 Å root-mean-square deviation of the superposition of the Cα atoms of residues 2−40 and 104−141 of dCD onto the corresponding residues of the N-terminal domain of CDA-D (residues 49−89 and 102−138, respectively) indicates a high degree of similarity in the cores of the molecules, despite differences in the folds (as described above). In addition to the conserved catalytic residues, most of the other residues that interact with the base and ribose group of the inhibitor are conserved (Figure 5c). Most interestingly, the side chain of Tyr153 of dCD, which interacts with the phosphate group and with the base, is replaced with Phe165 of the second subunit in CDA, where it stacks against the base in a similar manner and presumably has a similar role in defining the substrate specificity. If the residues involved in binding the phosphate group in dCD or the 5′-hydroxyl in CDA are not counted, there is only one residue involved in substrate binding that is different between the two enzymes. Glu91 of CDA makes

a hydrogen bonding contact with O3′ of the ribose. Surprisingly, this residue has been shown to be important not only for substrate binding but also for catalytic activity (*36*). dCD does not have a corresponding residue, and this area is occupied by residues that are mainly important for the binding of the phosphate group. The histidine that binds the catalytically important zinc ion has a somewhat different conformation in the two structures (Figure 5c). This difference appears to be related to the presence (CDA) or absence (dCD) of the 2′-hydroxyl on the ribose and a difference in the orientation of the ribose relative to the base and thus represents an adaptation to the differences in the composition of the inhibitors.

Despite differences in their substrate-binding sites, the biochemical data and the similarities in their respective active sites suggest that the catalytic mechanisms of dCD and CDA are essentially identical. This idea is further supported by the fact that the analogous inhibitors, PdR for dCD and zebularine for CDA (*37*), are found in identical hydrated states in the respective active sites. Furthermore, while the ligand of dCD is bound in a slightly different orientation in the binding cleft and the ribose ring is in a conformation different from that of the zebularine derivative in CDA-D, their bends at the N1−C1′ glycosidic link are similar (Figure 5c). An increase in the angle of this bend along the reaction pathway was observed for CDA-D, based on the structures of complexes with a series of ligands that correspond to the substrate, the intermediate state, and the product. This increasing distortion of the ligand, combined with a shift of the pyrimidine toward the catalytic zinc ion, was proposed to constitute a "spring-loading" effect, facilitating release of the product at the end of the reaction (*38*).

Nevertheless, subtle differences in the geometries of the active sites of dCD, CDA-D, and CDA-T indicate that small variations among the respective mechanisms of the enzymes are possible. Most interestingly, the distance between O4 of the hydrated pyrimidine and the zinc ion is different: 1.95 Å in CDA-D and 2.20 Å in dCD. Likewise, the distance between the zinc ion and Cys135 is longer (2.38 Å) in the dCD structure than the corresponding zinc−Cys132 distance in CDA-D (2.20 Å). This may be important because changes in the distance to Cys132 in the different complexes of CDA-D were proposed to be related to its role as the valence buffer (*39*). However, the zinc ion coordination distances of dCD are similar to those observed in the CDA-T structure, which lacks the active site histidine but instead has three cysteines coordinating the zinc ion. In addition, the conformation of the side chain of His104 in dCD is also not identical to that of His102 in CDA-D. This appears to be related to the absence of the O2′ hydroxyl in the ligand of dCD and may be significant, because of the apparent role of the interaction with the ribose ring in the stabilization of the reaction intermediates in CDA (*36*).

DISCUSSION

Subunit Interaction and Potential Regulatory Site. It is proposed that the T4-dCD-R115E dimer in solution consists of molecules A and B while the hexamer observed in the crystal structure, and consequently the interaction across the AC interface, is produced during the crystallization process. Protein aggregation into the hexamer becomes favorable when the local protein concentration becomes extremely high in an environment that also has high salt concentrations. Although the surface areas of both interfaces are similar, the AB interface with its central two-helix bundle appears to be the more stable one and thus the one present in the dimer. Furthermore, the side chains of Glu115 of molecule A and Glu121 of molecule C are sufficiently close that an Arg at position 115, as it is in the wild-type protein, could easily form a salt bridge interaction with Glu121. Thus, it is likely that the R115E mutation eliminates an attractive interaction at this location on the AC interface, which would at least be a contributing factor to the destabilization of the hexamer. The existence and the proposed function of this salt bridge assume that the AC interface and the hexamer seen in the crystal are similar to the AC interface and the hexamer, respectively, of the wild-type enzyme. This concept is supported by the fact that the AC interface has all the characteristics of a typical subunit interface, including a core of hydrophobic contacts surrounded by polar interactions. Furthermore, Phe112 and Glu115 are located in a pocket at the subunit interfaces and close to the core of the hexamer. The location and characteristics of this pocket are consistent with it being the binding site of the allosteric regulators. It is formed by several, mostly polar, residues from three subunits (A−C) (Figure 6). Residues Phe112 and Glu115 are located at the bottom of the pocket where the side chain of Phe112 stacks against the hydrophobic section of the side chain of Arg33 of molecule B and Glu115 is close to residue 121 of molecule C.

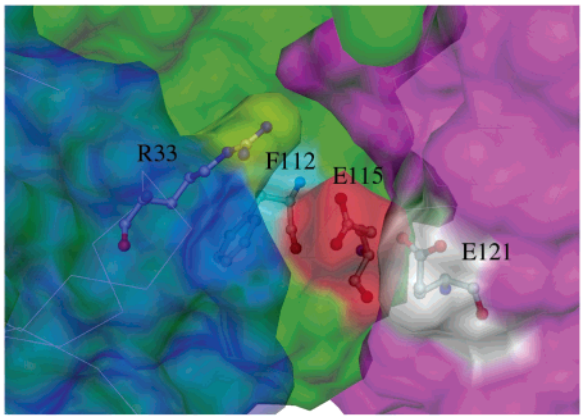

FIGURE 6: Subunit−subunit interaction and regulatory site. Detailed surface representation of the subunit−subunit interactions near the residues that are known to be important for the binding of the allosteric regulators. The same color scheme is used as in the hexamer in Figure 3b. Residues Phe112 (cyan) and Glu115 (red) of molecule A (green) are located in a pocket that is formed between the three subunits. Phe112 stacks with Arg33 (yellow) of molecule B (blue). Glu115 is near Glu121 (white) of molecule C (magenta). In the wild-type enzyme, Arg115 and Glu121 would be sufficiently close to form a salt bridge, stabilizing the subunit association. This figure was prepared with DINO (*45*).

Activity of T4-dCD-R115E and Proposed Model for Allosteric Regulation of Wild-Type T4-dCD. The absence of the interactions involving molecule C in the dimer of T4-dCD-R115E in solution leads to an explanation of how the mutant can be active in the absence of dCTP. In an AB dimer, the ligand in the substrate-binding site is not more exposed than it is in the hexamer, but the structural elements that form the binding site, especially α-helix 3, are less constrained and probably are capable of movement to allow

entry of the ligands. This requirement for movement of structural elements that form the substrate-binding site is not too different from the mechanism of CDA, which has a binding site very similar in structure. However, the structural elements that form the substrate-binding site of CDA, which is fully sequestered between subunits, are contributed by multiple subunits. In this case, entry of the substrate would require separation of the subunits at the interface, which is an allosterically controlled process. Thus, we can conclude that T4-dCD-R115E is incapable of binding the allosteric regulators, due to the incompleteness of the binding pocket. However, it is active as a dimer because it has the conformational flexibility required for the entry and exit of the substrate.

Furthermore, if we again assume that the hexamer resembles the hexamer of the wild-type enzyme, it is possible to develop a model for the allosteric activation of the enzyme. The pocket that contains residues 112 and 115 is distant from, and on the surface opposite from, the substrate-binding site, but at the subunit interfaces. This location is typical for the regulatory site of an enzyme that is allosterically regulated by heterotropic effects (*40*, *41*). Since it is known that activation of wild-type dCD by dCTP involves conformational changes at the subunit interface (*10*), we propose that binding of dCTP alters the AC interface to reduce the restraint on the structural elements that form the substrate-binding site, resulting in enzyme activation.

ACKNOWLEDGMENT

The use of the ultracentrifuge facility of the Biochemistry Shared Instrumentation Core at the Wadsworth Center is gratefully acknowledged.

REFERENCES

1. Maley, F., and Maley, G. F. (1999) Structure, function analysis of T4-phage dexoycytidylate deaminase and its role in the phage metabolic pathway, *Paths Pyrimidines 7*, 1−7.
2. Nicander, B., and Reichard, P. (1985) Evidence for the involvement of substrate cycles in the regulation of deoxyribonucleoside triphosphate pools in 3T6 cells, *J. Biol. Chem. 260*, 9216−9222.
3. Carreras, C. W., and Santi, D. V. (1995) The catalytic mechanism and structure of thymidylate synthase, *Annu. Rev. Biochem. 64*, 721−762.
4. Rose, M. G., Farrell, M. P., and Schmitz, J. C. (2002) Thymidylate synthase: a critical target for cancer chemotherapy, *Clin. Colorectal Cancer 1*, 220−229.
5. Maley, F., and Maley, G. F. (1972) in *Current Topics in Cellular Regulation* (Horecker, B. L., and Stadtman, E. R., Eds.) pp 177−228, Academic Press, New York.
6. Hernandez-Santiago, B., Placidi, L., Cretton-Scott, E., Faraj, A., Bridges, E. G., Bryant, M. L., Rodriguez-Orengo, J., Imbach, J. L., Gosselin, G., Pierra, C., Dukhan, D., and Sommadossi, J. P. (2002) Pharmacology of β-L-thymidine and β-L-2′-deoxycytidine in HepG2 cells and primary human hepatocytes: relevance to chemotherapeutic efficacy against hepatitis B virus, *Antimicrob. Agents Chemother. 46*, 1728−1733.
7. Liou, J.-Y., Krishnan, P., Hsieh, C.-C., Dutschman, G. E., and Cheng, Y.-C. (2003) Assessment of the effect of phosphorylated metabolites of anti-human immunodeficiency virus and anti-hepatitis B virus pyrimidine analogs on the behavior of human deoxycytidylate deaminase, *Mol. Pharmacol. 63*, 105−110.
8. Maley, F. (1962) Nucleotide interconversions. VII. The effect of halogenated and *N*-methyl derivatives of deoxycytidylic acid on deoxycytidylate deaminase and thymidylate synthetase, *Biochim. Biophys. Acta 60*, 135−138.
9. Neuhard, J., and Nygaard, P. (1987) in *Purines and pyrimidines* (Neidhardt, F. C., Ingraham, J. L., Low, K. B., Magasanik, B., Schaechter, M., and Umbarger, H. E., Eds.) pp 445−473, American Society for Microbiology, Washington, DC.
10. Maley, G. F., and Maley, F. (1982) Allosteric transitions associated with the binding of substrate and effector ligands to T2 phage induced deoxycytidylate deaminase, *Biochemistry 21*, 3780−3785.
11. Anderson, A. C., O'Neil, R. H., DeLano, W. L., and Stroud, R. M. (1999) The structural mechanism for half-the-sites reactivity in an enzyme, thymidylate synthase, involves a relay of changes between subunits, *Biochemistry 38*, 13829−13836.
12. Maley, F., Pederson-Lane, J., and Changchien, L. M. (1995) Complete restoration of activity to inactive mutants of *Escherichia coli* thymidylate synthase: evidence that *E. coli* thymidylate synthase is a half-the-sites activity enzyme, *Biochemistry 34*, 1469−1474.
13. McGaughey, K. M., Wheeler, L. J., Moore, J. T., Maley, G. F., Maley, F., and Mathews, C. K. (1996) Protein−protein interactions involving T4 phage-coded deoxycytidylate deaminase and thymidylate synthase, *J. Biol. Chem. 271*, 23037−23042.
14. Maley, G. F., Lobo, A. P., and Maley, F. (1993) Properties of an affinity-column-purified human deoxycytidylate deaminase, *Biochim. Biophys. Acta 1162*, 161−170.
15. Moore, J. T., Ciesla, J. M., Changchien, L. M., Maley, G. F., and Maley, F. (1994) Identification of a site necessary for allosteric regulation in T4-phage deoxycytidylate deaminase, *Biochemistry 33*, 2104−2112.
16. Keefe, R. G., Maley, G. F., Saxl, R. L., and Maley, F. (2000) A T4-phage deoxycytidylate deaminase mutant that no longer requires deoxycytidine 5′-triphosphate for activation, *J. Biol. Chem. 275*, 12598−12602.
17. Betts, L., Xiang, S., Short, S. A., Wolfenden, R., and Carter, C. W. J. (1994) Cytidine deaminase. The 2.3 Å crystal structure of an enzyme: transition-state analog complex, *J. Mol. Biol. 235*, 635−656.
18. Carlow, D. C., Carter, C. W. J., Mejlhede, N., Neuhard, J., and Wolfenden, R. (1999) Cytidine deaminases from *B. subtilis* and *E. coli*: compensating effects of changing zinc coordination and quaternary structure, *Biochemistry 38*, 12258−12265.
19. Snider, M. J., Gaunitz, S., Ridgway, C., Short, S. A., and Wolfenden, R. (2000) Temperature effects on the catalytic efficiency, rate enhancement, and transition state affinity of cytidine deaminase, and the thermodynamic consequences for catalysis of removing a substrate "anchor", *Biochemistry 39*, 9746−9753.
20. Reizer, J., Buskirk, S., Bairoch, A., Reizer, A., and Saier, M. H., Jr. (1994) A novel zinc-binding motif found in two ubiquitous deaminase families, *Protein Sci 3*, 853−856.
21. Johansson, E., Mejlhede, N., Neuhard, J., and Larsen, S. (2002) Crystal structure of the tetrameric cytidine deaminase from *Bacillus subtilis* at 2.0 Å resolution, *Biochemistry 41*, 2563−2570.
22. Johansson, E., Neuhard, J., Willemoes, M., and Larsen, S. (2004) Structural, kinetic and mutational studies of the zinc ion environment in tetrameric cytidine deaminase, *Biochemistry 43*, 6020−6029.
23. Moore, J. T., Uppal, A., Maley, F., and Maley, G. F. (1993) Overcoming inclusion body formation in a high-level expression system, *Protein Expression Purif. 4*, 160−163.
24. Lebowitz, J., Lewis, M. S., and Schuck, P. (2002) Modern analytical ultracentrifugation in protein science: A tutorial review, *Protein Sci. 11*, 2067−2079.
25. Schuck, P., Perugini, M. A., Gonzalez, N. R., Howlett, G. J., and Schubert, D. (2002) Size-distribution analysis of proteins by analytical ultracentrifugation: strategies and application to model systems, *Biophys. J. 82*, 1096−1111.
26. Terwilliger, T. C., and Berendzen, J. (1999) Automated structure solution for MIR and MAD, *Acta Crystallogr. D55*, 849−861.
27. Cowtan, K. D., and Main, P. (1996) Phase combination and cross validation in iterated density-modification calculations, *Acta Crystallogr. D52*, 43−48.
28. Roussel, A., and Cambillau, C. (1989) in *Silicon Graphics Geometry Partners Directory* (Graphics, S., Ed.) pp 77−78, Silicon Graphics, Mountain View, CA.
29. Jones, T. A., Zou, J. Y., Cowan, S. W., and Kjeldgaard, M. (1991) Improved methods for the building of protein models in electron-density maps and the location of errors in these maps, *Acta Crystallogr. A47*, 110−119.
30. Brunger, A. T., Adams, P. D., Clore, G. M., DeLano, W. L., Gros, P., Grosse-Kunstleve, R. W., Jiang, J.-S., Kuszewski, J., Nilges, M., Pannu, N. S., Read, R. J., Rice, L. M., Simonson, T., and Warren, G. L. (1998) Crystallography and NMR system: a new

software suite for macromolecular structure determination, *Acta Crystallogr. D54*, 905−921.
31. Laskowski, R. A., McArthur, M. W., Moss, D. S., and Thornton, J. M. (1993) PROCHECK: a program to check the stereochemical quality of protein structures, *J. Appl. Crystallogr. 26*, 282−291.
32. Maley, G. F., MacColl, R., and Maley, F. (1972) T2r+ bacteriophage-induced enzymes. II. The subunit structure of deoxycytidylate deaminase, *J. Biol. Chem. 247*, 940−945.
33. Maley, G. F., and Maley, F. (1966) The significance of the substrate specificity of T2r+-induced deoxycytidylate deaminase, *J. Biol. Chem. 241*, 2176−2177.
34. Ireton, G. C., McDermott, G., Black, M. E., and Stoddard, B. L. (2002) The structure of *Escherichia coli* cytosine deaminase, *J. Mol. Biol. 315*, 687−697.
35. Johansson, E., Bjornberg, O., Nyman, P. O., and Larsen, S. (2003) Structure of the bifunctional dCTP deaminase-dUTPase from *Methanocaldococcus jannaschii* and its relation to other homotrimeric dUTPases, *J. Biol. Chem. 278*, 27916−27922.
36. Carlow, D. C., Short, S. A., and Wolfenden, R. (1998) Complementary truncations of a hydrogen bond to ribose involved in transition-state stabilization by cytidine deaminase, *Biochemistry 37*, 1199−1203.
37. Xiang, S., Short, S. A., Wolfenden, R., and Carter, C. W. J. (1995) Transition-state selectivity for a single hydroxyl group during catalysis by cytidine deaminase, *Biochemistry 34*, 4516−4523.
38. Xiang, S., Short, S. A., Wolfenden, R., and Carter, C. W. J. (1997) The structure of the cytidine deaminase-product complex provides evidence for efficient proton transfer and ground-state destabilization, *Biochemistry 36*, 4768−4774.
39. Xiang, S., Short, S. A., Wolfenden, R., and Carter, C. W. J. (1996) Cytidine deaminase complexed to 3-deazacytidine: a "valence buffer" in zinc enzyme catalysis, *Biochemistry 35*, 1335−1341.
40. Helmstaedt, K., Krappmann, S., and Braus, G. H. (2001) Allosteric regulation of catalytic activity: *Escherichia coli* aspartate transcarbamoylase versus yeast chorismate mutase, *Microbiol. Mol. Biol. Rev. 65*, 404−421.
41. Koshland, D. E. J. (1969) in *Current Topics in Cellular Regulation* (Horecker, B. L., and Stadtman, E. R., Eds.) pp 1−27, Academic Press, New York.
42. Esnouf, R. M. (1999) Further additions to MolScript version 1.4, including reading and contouring of electron-density maps, *Acta Crystallogr. D55*, 938−940.
43. Kraulis, P. J. (1991) MOLSCRIPT: a program to produce both detailed and schematic plots of protein structures, *J. Appl. Crystallogr. 24*, 946−950.
44. Merritt, E. A., and Bacon, D. J. (1997) Raster3D: photorealistic molecular graphics, *Methods Enzymol. 277*, 505−524.
45. DINO (2001) http://www.dino3d.org.

BI048928H